

Effect of boundary layer low-level jet on fog fast spatial propagation

Shuqi Yan¹, Hongbin Wang^{1,*}, Xiaohui Liu², Fan Zu¹, Duanyang Liu^{1,*}

¹Key Laboratory of Transportation Meteorology of China Meteorological Administration, Nanjing Joint Institute for Atmospheric Sciences, Nanjing, 210041, China

²Merchant Marine College, Shanghai Maritime University, Shanghai, 201306, China

Correspondence to: Hongbin Wang (kaihren@163.com); Duanyang Liu (liuduanyang2001@126.com)

Abstract. The spatiotemporal variation of fog reflects the complex interactions among fog, boundary layer thermodynamics and synoptic systems. Previous studies revealed that fog can present fast spatial propagation feature and attribute it to boundary layer low-level jet (BLLJ), but the effect of BLLJ on fog propagation is not quantitatively understood. Here we analyze a large-scale fog event in Jiangsu, China from 20 to 21 January 2020. Satellite retrievals show that fog propagates from southeast coastal area to northwest inland with the speed of 9.6 m/s, which is three times larger than the ground wind speeds. The ground meteorologies are insufficient to explain the fog fast propagation, which is further investigated by WRF simulations. The fog fast propagation could be attributed to the BLLJ occurring between 50 and 500 m, because the wind speeds (10 m/s) and directions (southeast) of BLLJ core are consistent with fog propagation. Through sensitive experiments and process analysis, three possible mechanisms of BLLJ are revealed: 1) The abundant oceanic moisture is transported inland, increasing the humidity of boundary layer and promoting condensation; 2) The oceanic warm air is transported inland, enhancing the inversion layer and favouring moisture accumulation; 3) The moisture advection probably promotes ~~upper-level fog~~ low stratus formation, and later it subsides to be ground fog by turbulent mixing of fog droplets. The fog propagation speed would decrease notably by 6.4m/s (66%) in the model if the BLLJ-related moisture and warm advections are turned off.

1. Introduction

Fog is a kind of low-visibility weather phenomenon that occurs at near surface, causing adverse impacts on traffic transportation. The formation, development and dissipation of fog are the comprehensive results of the interactions among radiation, moisture, microphysics, turbulence, aerosols and other factors (Gultepe et al., 2007; Koraćin et al., 2014; Nakanishi, 2000). The relations of fog with meteorological factors are highly variable under different conditions. Therefore, the mechanism of fog evolution needs to be intensively studied.

Under favourable conditions, the fog intensity or its spatial extent can develop extraordinarily fast with time. Field observations conducted at single site reveal that visibility in fog can deteriorate drastically, from about 1km to less than 200m within 30min (Li et al., 2019). It is referred to as fog burst reinforcement, which is firstly raised by Korb et al. (1970) and systematically reviewed by Liu et al. (2012) and Li et al. (2019). Fog burst reinforcement is accompanied by the drastic formation of fog droplets, sudden increase of fog liquid water and broadening of droplet spectrum (Liu et al., 2017; Liu et al., 2021). Additionally, fog can develop rather fast in spatial extent, i.e., the fast spatial propagation of fog (Zhu et al., 2022). It is reflected by the successive visibility dropping in space along a certain direction. The influencing factors of fast

35 spatial propagation could be more complex than that of the burst reinforcement at single site, which have received fewer
36 quantitative studies recently.

37 Synoptic systems and planetary boundary layer (PBL) thermodynamic structures are key to understanding the cause of fog
38 burst reinforcement and fast propagation. Weak cold air invasion and radiative cooling is an important factor for fog burst
39 reinforcement and fast propagation (Liu et al., 2011; Wang et al., 2020). Dhangar et al. (2021) demonstrated that the radiative
40 cooling at surface and fog top can increase supersaturation and promote fog vertical development. Shen et al. (2022)
41 found that the different cooling rates at two nearby stations lead to a remarkable difference in fog formation time, fog du-
42 ration and vertical extent. Sufficient water supply is also an important factor. Wobrock et al. (1992) revealed that the role
43 of moisture advection outweighs radiative cooling in large-scale fog events. Pu et al. (2008) found that two layers of mois-
44 ture advection enhance fog development and maintenance. Under stable synoptic systems, the PBL thermodynamic can
45 also favour fog burst reinforcement and fast fog propagation. The formation of dense fog is usually accompanied by strong
46 inversion layer, of which the intensity could reach 16K/100m (Pu et al., 2008; Liu et al., 2012). Liu et al. (2016) found that
47 upper-level warm advection and low-level cold advection significantly enhance inversion intensity and promote fog de-
48 velopment. The vapor advection resulting from southerly winds further increases fog intensity. Appropriate turbulence also
49 facilitates fog formation and enhancement (Ye et al., 2015; [Zhou and Ferrier, 2008](#)). Turbulent results in the exchange of
50 heat and moisture within PBL, e.g., the downward entrainment of vapor and cold air can promote condensation and droplet
51 formation (Liu et al., 2016; Zhang et al., 2005). Other studies highlight the role of hygroscopic aerosols and aerosol indi-
52 rect effects in strong fog events (Boutle et al., 2017; Quan et al., 2021; Shao et al., 2023; Wang et al., 2023; Yan et al.,
53 2021).

54 Previous studies find that the large-scale fog events are accompanied by boundary layer low-level jet (BLLJ), and try to
55 attribute the spatial propagation of fog to BLLJ. The causes of BLLJ include such as synoptic systems, terrain effect and
56 inertial oscillation (Kraus et al., 1985). Tian et al. (2019) demonstrated that the warm-and-wet southerly BLLJ favours wa-
57 ter vapor transportation and inversion layer construction, and later the fog is triggered by a weak cold front invasion. Wu et
58 al. (2020) found that strong northerly BLLJ associated with cold air can destroy inversion layer and lead to early dissipa-
59 tion of fog, while weak BLLJ can promote fog maintenance. Li et al. (2012) revealed that the strengthened turbulence gen-
60 erated by BLLJ wind shear promotes vertical mixing and facilitates fog development. However, the relations between
61 BLLJ and fog propagation and the key synoptic factors have not been quantitatively addressed. Also, the current horizontal
62 and vertical observations are not sufficient to reveal the mechanism of fog propagation. It requires further investigation by
63 numerical models.

64 In this work, we study a large-scale fog event with fast propagation feature occurring in Jiangsu Province, China from 20
65 to 21 January 2020. By combination of observations and numerical simulations, we aim to quantitatively reveal the BLLJ
66 effect on fast fog propagation to and identify the key impact factors and mechanisms. This work is expected to better un-
67 derstand the complex interactions among synoptic systems, PBL thermodynamics and fog spatial propagation, as well as
68 provide prediction indicators for operational fog forecast. The study is organized as follows: Section 2 describes the data,
69 methods and numerical models of this study. Sections 3.1 to 3.4 analyze the fog propagation feature and PBL characteris-

70 tics. Section 3.5 quantitatively study the BLLJ effect on fast fog propagation and identifies key influencing factors. Section
71 4 concludes the findings of this study.

72 **2. Data, methods and model configuration**

73 **2.1 Data and study area**

74 This study focuses on the Jiangsu area, China (Figure 1), where a large-scale fog event occurred from 20 to 21 January
75 2020. We collected the data from 70 ground automatic weather stations (AWS) in Jiangsu Province, China. The data is
76 recorded by every 10 minutes, including visibility, temperature, relative humidity (RH), wind direction and wind speed.
77 This data is used to analyze the temporal variation of meteorology, as well as evaluate the model performance on tempera-
78 ture, RH and wind. Additionally, the Sheyang (SY; 120.25°E, 33.76°N; 3m) station is a sounding station that used for
79 model evaluation in the vertical direction. The sounding observations include temperature, RH, wind direction and wind
80 speed which are sampled each second. It is conducted twice a day (00UTC and 12UTC).

81 The geostationary satellite Himawari 8 (<https://www.eorc.jaxa.jp/ptree/index.html>) is used to retrieve nighttime fog area
82 and evaluate the model performance of fog simulation. The high spatiotemporal resolution (2km in space and 1h in time) is
83 suitable for detecting the fast evolution of fog area. This satellite observation includes 16 bands, and the bands at 3.9 and
84 11.2 μm are used.

85 The ERA5 reanalysis data (<https://cds.climate.copernicus.eu/cdsapp#!/dataset/reanalysis-era5-pressure-levels>) is used to
86 analyze synoptic conditions and provide initial & boundary fields for model simulation. The grid resolution is 0.125°
87 (about 12.5km) and the time interval is 6h. All the time in this study is local time (UTC+8).

88 **2.2 Methods**

89 2.2.1 Satellite fog retrieval

90 Since the ground AWS stations are not sufficiently fine in spatial resolution, the high spatiotemporal resolution product of
91 Himawari 8 is suitable to study the propagation of fog. Nighttime fog has notable different optical properties at the bands
92 of 3.9 μm and 11.2 μm , so it can be indicated by the dual-band brightness temperature difference ($T_{bb_{3.9}}$ minus $T_{bb_{11.2}}$)
93 lower than a threshold (Cermak et al., 2008). In this study, the threshold is determined to be -2 K following the dynamic
94 threshold algorithm proposed by Di Vittorio et al. (2002). Daytime fog after 08:00 is not retrieved because we mainly fo-
95 cus on the formation and development stage of fog before 08:00.

96 2.2.2 Fog propagation speed calculation

97 We calculate the propagation speed according to satellite retrieved fog area. At 22:00 on 20 January 2020, a tiny fog area
98 appeared at Nantong and Yanchen coastal region with an area smaller than 50km² (figure not shown). The center of this
99 fog area is set as point A (120.6°E, 32.9°N). We draw a line starting from A with an arbitrary direction, and find its inter-
100 section with the fog boundary area at 07:00 next day (point B). Then the propagation speed in this direction can be calcu-

101 lated by the distance from A to B divided by 9 hours (22:00~07:00). By looping from 0 to 360 with the interval of 1°,
102 propagation speeds in all directions are calculated, and the maximum speed is defined as the fog propagation speed.

103 The fog propagation speed is verified by AWS data. We select three representative stations along the fog propagation di-
104 rection, Dafeng (DF; 120.48°E, 33.20°N, 14m), Baoying (BY; 119.30°E, 33.23°N, 15m), Sihong (SH; 118.22°E, 33.48°N,
105 13m) (Figure 1). According to their distances and the time differences when visibility drops to 200m, the propagation
106 speed between two adjacent stations is calculated.

107 2.2.3 Process analysis on fog

108 The simulated fog is indicated by fog liquid water content (LWC). Process analysis is used to quantify the contribution of
109 each physical process to LWC variation (Schwenkel et al., 2019; Yan et al., 2020). The variation of LWC is related to the
110 following terms:

$$111 \quad \frac{\partial \text{LWC}}{\partial t} = - \underbrace{\left(u \frac{\partial}{\partial x} + v \frac{\partial}{\partial y} + w \frac{\partial}{\partial z} \right)}_{\text{Adv}c} \text{LWC} + \left(\frac{\partial \text{LWC}}{\partial t} \right)_{\text{Vmix}} + \left(\frac{\partial \text{LWC}}{\partial t} \right)_{\text{Cond}} + \left(\frac{\partial \text{LWC}}{\partial t} \right)_{\text{Sedi}} + \left(\frac{\partial \text{LWC}}{\partial t} \right)_{\text{other}}$$

112 where Advc includes horizontal and vertical advection, Vmix is associated with the fog droplet vertical exchange by tur-
113 bulent mixing, Cond is the vapor condensation (negative means droplets evaporation), Sedi is fog droplets sedimentation.
114 Other microphysical processes include autoconversion, accretion and cold phase processes. They are much smaller than the
115 previous four processes, so they can be safely ignored.

116 2.3 Model configuration and experiments

117 The Weather Research and Forecasting model (WRF) is implemented to study the fast spatial propagation of fog events.
118 Two domains are set up (Figure 1). The parent domain covers East China, with the grid size of 181×181 and grid interval
119 of 9 km. The nested domain covers Jiangsu Province and its coastal area, with the grid size of 199×199 and grid interval of
120 3 km. To simulate the turbulent process more reasonably, the vertical levels are refined to 42 levels, with 25 levels under
121 1500m and 9 levels under 100m (Yang et al., 2019; Yan et al., 2020). The first model level is about 4m. The model is driv-
122 en by the initial and boundary field from ERA5 Reanalysis. The simulation starts at 08:00 on 19 January and ends at 08:00
123 on 21 January 2020, with the first 24h as spin-up period. All the time in this study is local time (UTC+8).

124 Fog is hard to be simulated or predicted well (Zhou et al., 2010, 2012), which simulation is sensitive to the choice of pa-
125 rameterization schemes (Steenefeld et al., 2014; van der Velde et al., 2010). Through massive tests, the QNSE boundary
126 layer scheme (Sukoriansky et al., 2005) and Pleim-Xiu land surface scheme (Pleim et al., 2009) yield the best simulation
127 performance. Other parameterization schemes are listed in Table 1. The simulated fog is indicated by the liquid water con-
128 tent (LWC) greater than 0.015g/kg under the height of 500m, which corresponds to horizontal visibility less than 1km
129 (Kunkel, 1983).

130 Apart from the base experiment, three sensitive experiments are performed to elucidate the mechanism of fast fog propa-
131 gation (Table 1). The experiment "Tadv0" turns off the temperature advection within PBL during the fog period. The ex-

132 periment "QvAdv0" and "QcAdv0" are the same as "Tadv0" except that turning off water vapor advection and ~~fog-cloud~~
133 water advection, respectively. The experiment "NoAdv" turns off all the advections above. Therefore, the differences of the
134 base experiment with Tadv0, QvAdv0, and Qcadv0 represent the effect of temperature advection, moisture advection, and
135 ~~fog-cloud~~ water advection, respectively. The reasons and results of the sensitive experiments will be discussed in Section
136 3.5.

137 3. Results

138 3.1 Fog overview and synoptic background

139 The studied fog event occurs at the night of 20 January and dissipates in the daytime of 21 January 2020 (Figure 2). Figure
140 3 shows the synoptic situations at 08:00 and 20:00 on 20 January. At 500hpa, a frontal zone is located north of 38°N. The
141 Jiangsu area is dominated by prevailing westerly flows with no obvious troughs. At 850hpa, a ridge moves eastward and
142 controls Jiangsu area. The descending motions associated with the ridge and the nocturnal radiative cooling at ground fa-
143 vour the establishment of inversions. At ground level, a weak cold high pressure moves eastward with the central pressure
144 of 1030hpa. The Jiangsu area is dominated by uniform pressure field with small wind speeds, which strengthens atmos-
145 pheric stratification stability and promotes the accumulation of aerosols and moisture. The moisture condition in Jiangsu is
146 additionally favoured by the water vapor transportation from ocean by easterly winds at 20:00. Under this conductive situ-
147 ation, the fog event occurred from nighttime of 20 to daytime of 21 January over Jiangsu Province (Figure 2).

148 3.2 Fog and ground meteorology variation

149 Hourly Himawari 8 satellite image clearly shows the spatial propagation of fog (Figure 2). The fog initials at 22:00 on 20
150 January in Nantong and Yanchen coastal region with an area smaller than 50km². Later, this small fog area expands to a
151 large-scale fog. Specifically, the southeast side of fog area varies relatively slowly, but the northwest side expands re-
152 markably, indicating a large propagation speed. At 07:00 on 21 January, the front of fog expands to Anhui Province. After
153 07:00, the fog begins to dissipate, and it fully disappears at 11:00 (figure not shown). Figure 4 quantitatively describes the
154 propagation direction and speed of fog. From the east to south directions (the fourth quadrant), fog propagation speed is
155 less than 3m/s. In the west-northwest and west directions, fog propagation speed is larger than 6m/s, and the maximum
156 propagation speed is 9.6m/s occurring at 160° direction (in Cartesian coordinate system). The fast propagation of fog is
157 also reported previously in Jiangsu area (Gao et al., 2023; Zhu et al., 2022), where the fog propagates from coastal area to
158 west boundary of Jiangsu within about 10h.

159 Visibilities at three representative stations, Dafeng (DF), Baoying (BY) and Sihong (SH) are used to verify the fog propa-
160 gation speed calculated by satellite (Table 2; Figure 5). At DF, fog forms (visibility less than 1km) early at 19:45 on 20
161 January. The visibility drops sharply at 23:15 and reaches the minimum at about 00:15. At BY and SH, fog forms in turn,
162 and their visibilities also have burst decreasing feature at 03:40 and 07:00, respectively. We calculate the fog propagation
163 speed by the distances among stations and the time differences when visibility drops to 200m. The propagation speed is 7.6

164 m/s between DF and BY and 8.3 m/s between BY and SH. These values correspond to the speed calculated by satellite
165 observation.

166 Figure 5 shows the variation of other meteorological fields. We focus on the characteristics from fog formation to the burst
167 visibility dropping (indicated by yellow dashed lines). At DF, the northerly wind decreases to lower than 1.5m/s at fog
168 formation, which causes the weak cold advection and temperature decreasing. The temperature keeps decreasing and fa-
169 vours the burst reduction of visibility at 23:15. The vapor content (indicated by dew point) increases sharply before 17:00
170 and decreases slightly since then, so the RH increasing after fog formation is caused by temperature drop. At BY and SH,
171 the wind directions are dominantly southeast and the speeds are generally less than 2m/s before fog formation. The tem-
172 perature keeps decreasing and vapor content keeps increasing, leading to the further reduction of visibility. Later, the
173 southeasterly winds obviously enhance by about 1m/s, which may contribute to the burst visibility dropping due to the in-
174 tensified vapor advection from ocean.

175 The preliminary cause of fog formation and intensification are summarized. As located near the ocean, the moisture at DF
176 reaches the maximum prior to fog formation, so the fog formation and intensification are largely caused by radiative cool-
177 ing and weak cold advection. At BY and SH, the temperature cooling rate is weaker than DF, which is partly due to the
178 weak warm advection by southeasterly winds. The vapor advection by southeasterly winds favours fog development, and
179 the burst decrease in visibility coincides with the increase in wind speed. Therefore, deduced from BY and SH, the vapor
180 transportation associated with southeasterly winds could be an important reason for northwesterly propagation of fog.
181 However, it is obvious that the ground wind speed is rather small compared with fog propagation speed. Statistics on AWS
182 stations show that although wind direction (east, southeast and south winds at 70% stations) is generally in accordance
183 with fog propagation direction, wind speed is lower than 3m/s at 97% stations from 22:00 to 07:00, which is about
184 one-third of the fog propagation speed. Therefore, the ground meteorological field is insufficient to explain the fast propa-
185 gation of fog. The fog PBL characteristics and the key influencing factors need to be investigated by numerical simula-
186 tions.

187 3.3 Model evaluation

188 Figure 6a evaluates the model performance on temperature, relative humidity (RH) and wind field at surface. The simulat-
189 ed temperature and RH agree well with observations, with the root mean square error (RMSE) of 1.0K and 11%, respec-
190 tively. The simulation reasonably captures the wind direction transition from north to east, and the RMSE is less than 1m/s.

191 Figure 6b evaluates the model performance on temperature, RH and wind field in the vertical direction at SY sounding
192 station. The temperature profile is simulated well by the model, with the mean bias of less than 1K. The RH bias is rela-
193 tively small below about 200m, while it is a bit larger above 200m at 08:00 on 21 January. The simulated wind speed and
194 direction are basically consistent with observation. The large winds (greater than 6m/s) at about 200m are well reproduced
195 by the model, indicating that the model reasonably simulates boundary layer low-level jet. Studies on boundary layer
196 low-level jet are presented in next sections.

197 Figure 2 compares the satellite observed and simulated fog area. The simulation is only evaluated before 07:00, because
198 the dissipation of fog after 08:00 is not the focus in this study. The model reasonably captures the spatiotemporal evolution
199 of fog, with a slight overestimation of 5~10% in fog area.

200 Overall, the simulation reasonably captures the temporal variation of meteorology and reproduces the spatial propagation
201 of fog. It establishes the basis for discerning the mechanism of fog propagation.

202 **3.4 Characteristics of fog and PBL structure**

203 The thermodynamic variation of PBL is crucial for understanding the propagation of fog. Figure 7a shows the temporal
204 variation of horizontal winds in vertical directions. The simulated wind speed is consistently smaller than 4m/s under about
205 30m, while it remarkably increases with height. At 18:00 on 20 January, a large wind speed zone (>6m/s) forms at the
206 height between 50 and 500m in the east of 120°E. Since then, the large wind zone moves westward quickly accompanied
207 by wind speed increasing. During the fog period, the average wind speed exceeds 6m/s at the height between 50 to 500m
208 (Figure 7b), which is commonly larger than the wind speed in most fog events. Here, we refer to this large wind speed
209 zone as boundary layer low-level jet (BLLJ). The existence of BLLJ is supported by ERA5 reanalysis on 1000hpa and
210 975hpa levels (Figure 7b).

211 The formation of BLLJ is likely caused by the easterly movement of a high pressure at 1000hpa over East China. The cen-
212 tral pressure gets enhanced, which strengthens the pressure gradient over Jiangsu area and favours wind speed increasing
213 (figure not shown). The jet core (maximum wind speed) occurs at about 1000hpa (200m), with the time-averaged speed of
214 10m/s (Figure 7b). At that level, the dominant wind direction is southeast and the wind speed over fog area is 8~16m/s
215 (Figure 7c), which can fit the propagation direction and speed of fog. Also, the expansion speed of vertical fog zone is
216 comparable to the movement speed of jet core (Figure 7a). Therefore, we hypothesize that the southeasterly BLLJ could
217 account for the fast propagation of fog.

218 Previous studies reveal that southerly BLLJ can transport abundant water vapor to China inland and thus promote fog for-
219 mation (Liu et al., 2016; Tian et al., 2019). Figure 8 shows the temporal variation of water vapor mixing ratio (Q_v) profiles.
220 Since the vapor content over the ocean is higher, it is transported to inland areas by southeasterly BLLJ. The BLLJ can
221 further increases the Q_v in PBL by wind speed horizontal convergency and vertical shear. The larger wind speed in BLLJ
222 zone and lower wind speed outside BLLJ zone cause wind speed convergence, which favours the increase in PBL moisture.
223 Additionally, the turbulence generated by vertical shear of wind speed can promote vapor turbulent mixing, leading to the
224 higher Q_v above surface being entrained downward and increasing the ground Q_v (Gao et al., 2007). The Q_v under 300m
225 is generally higher than 3g/kg under the effect of BLLJ. Wu et al. (2020) also found that BLLJ continuously transports
226 water vapor to fog layer, resulting in surface Q_v higher than 3g/kg. It is notable that the expansion of vertical fog area co-
227 incides with the movement of the zone of $Q_v > 4\text{g/kg}$. Therefore, moister advection by BLLJ could be an important reason
228 for fast fog propagation.

229 BLLJ is reported to result in warm advection and deepen inversion layer previously (Tian et al., 2019), and inversion layer
230 is an important reason for fog burst reinforcement in most fog cases (e.g., Li et al., 2019; Liu et al., 2012; Jiao et al., 2016).

231 Figure 9 shows the temporal variation of temperature profile and inversion layer. The inversion layer here refers to the
232 height above ground where temperature monotonically decreases with height. Since 20:00 on 20 January, the ground tem-
233 perature keeps decreasing due to radiative cooling. Within the fog area, the temperature drop is more significant, which is
234 due to the longwave radiative cooling by fog droplets (Bott, 1991; Jia et al., 2018). Approximately above the fog top, there
235 is an obvious warm air mass transported from ocean to inland areas. The BLLJ-induced warm advection increases vertical
236 temperature gradient and strengthens atmospheric stability. Accordingly, the inversion height over non-fog areas basically
237 keeps increasing. The approximate inversion layer height is about 100~300m, which is consistent with previous studies
238 (Dorman et al., 2021; Li et al., 2019)., ~~with the~~ The maximum inversion intensity of 15K/100m, ~~which~~ ~~Such a strong in-~~
239 ~~version~~ is also reported in a dense fog event (16K/100m) by Pu et al. (2008). It favours the accumulation of vapor and
240 condensation nuclei, which is also a possible reason for fog formation in the downstream area.

241 Additionally seen from Figure 9, the west boundary of vertical fog region below about 100m has a negative slope, i.e., fog
242 forms at upper level ahead of forming at ground. The upper-level fog with no ground contact is referred to as low stratus.
243 The height at which fog/low stratus firstly forms is shown in Figure 10. An initial fog area forms at ground level before
244 00:00 on 21 January. Since then, low stratus ~~the majority of fog area firstly~~ forms at upper level (about 10~66m) over the
245 downstream area, while the ground fog in downstream area forms about 0~20min later than ~~upper-level fog~~ low stratus.
246 The formation of low stratus ~~upper-level fog~~ may also be caused by the BLLJ-induced moisture advection. In addition, the
247 fog-cloud water advection (Section 2.2.3) to downstream area by BLLJ could also be a potential reason. We hypothesize
248 that the formation of ground fog is partly favoured by the stratus lowering ~~subsidence of upper-level fog.~~ ~~Stratus lowering~~
249 ~~or upper fog subsidence to ground,~~ which has been reported by previous studies (e.g., Haeffelin et al., 2010; Liu et al.,
250 2012); the base height of stratus can be smaller than 100m before fog formation (Dupont et al., 2012; Fathalli et al., 2022),
251 which is basically close to our results (10~66m in Figure 10). While in this event, the stratus lowering phenomenon ~~up-~~
252 ~~per fog subsidence~~ remains to be verified by additional high-spatiotemporal resolution vertical observations.

253 According to above results, three potential factors for fog propagation are raised: BLLJ-related temperature advection,
254 moisture advection and fog-cloud water advection. These advectons possibly promote fog-low stratus formation ~~in the~~
255 ~~upper-level~~ within 100m above surface, and subsequently the low stratus ~~upper-level fog~~ could subside to be ground fog by
256 the turbulent mixing or sedimentation of fog-cloud droplets. Currently, their contributions to fog propagation have not been
257 quantitatively revealed. Therefore, it will be addressed in the next section.

258 3.5 Quantitative reasons for fast fog propagation

259 Four sensitive experiments, Tadv0, QvAdv0, QcAdv0 and NoAdv0 (Section 2.3) are conducted to quantify the respective
260 contributions of temperature advection, moisture advection, fog-cloud water advection and all these advectons to fog prop-
261 agation (Figure 11). Under the condition with no advectons (Figure 11a-d), there is a 80% decrease in fog area and a
262 6.4m/s (66%) decrease in propagation speed, which highlights the role of BLLJ-related advectons. When turning off tem-
263 perature advection (Tadv0) (Figure 11e-h), the original fog area in the base experiment shrinks 50% in size and breaks into
264 separate fog patches, and the propagation speed decreases by about 5.2m/s (54%). When turning off moisture advection
265 (QvAdv0) (Figure 11i-l), the fog area shrinks by 62% in size and the propagation speed decreases by about 4.6m/s (48%).

When turning off ~~fog-cloud~~ water advection (QcAdv0) (Figure 11m-p), the fog area nearly keeps unchanged during 00:00~04:00 and decreases moderately in size (about 25%) at 06:00. The propagation speed decreases moderately by 2.4m/s (25%). Deduced from the changes in fog area and propagation speed under various experiments, we can infer that the BLLJ-related warm and moisture advection, especially moisture advection, could be the major cause of fast spatial propagation, while ~~fog-cloud~~ water advection has a minor contribution.

We further perform process analysis on LWC (Section 2.2.3) to illustrate the mechanism of fog propagation (Figure 12). The horizontal and vertical values of Advc and Sedi are at least one order of magnitude smaller than that of Cond and Sedi, indicating that ~~fog-cloud~~ water transportation to downstream areas and droplet sedimentation to ground are not the causes of fog propagation. At 00:00 on ground level, Cond is positive over the newly formed fog area (blue and cyan colors surrounding the fog area), indicating that fog firstly forms at ground by radiative cooling before 00:00. After 02:00, Cond is almost negative over the entire fog area, indicating that fog does not firstly form at the ground level (otherwise Cond would have positive values). The formation of ground fog may be contributed by the LWC turbulent entrainment from upper level, because Vmix shows significant positive values after 02:00. In the vertical direction, Vmix and Cond are still two dominant physical processes (Figure 12b), and their signs show opposite patterns. At lower level (0~30m), Cond is negative and Vmix is positive, which is the same as their ground characteristics. At upper level (30~200m), Cond is positive and Vmix is negative instead, indicating that ~~fog-cloud~~ water is produced by vapor condensation at upper level and then being entrained to ground. The significant positive Cond supports that BLLJ-related moisture advection promotes vapor condensation and ~~fog-low stratus~~ formation ~~at upper level above surface~~, and the significant positive Vmix may indicate that the ~~low stratus upper level fog~~ favours ground fog formation by turbulent exchange of LWC.

4. Discussions

Previous studies have elucidated the qualitative reasons for fog propagation. In this study, we describe the feature of fast fog propagation and identify its key impact factors more quantitatively. Figure 13 summarizes the mechanism of fog propagation. During the nighttime, a southerly BLLJ controls the study region, and the jet core intensity is about 10m/s which occurs at about 200m. The ground fog propagates northwestward with the speed of 9.6m/s. The BLLJ favours the fast fog propagation by three possible mechanisms: 1) BLLJ transports sufficient vapor from ocean to inland area. The turbulence strengthened by wind speed shear further moistens the PBL and promotes vapor condensation. This could be the dominant mechanism. 2) BLLJ transports warmer air from ocean to inland area and deepens the inversion layer. The strengthened inversion favours the accumulation of vapor and condensation nuclei. 3) The strong moisture advection could promote the ~~upper level fog low stratus~~ formation in the downstream area, and later it subsides to ~~be ground fog~~ by turbulent exchange of ~~fog-cloud~~ droplets. The ~~stratus lowering phenomenon subsidence of upper level fog to ground~~ needs to be verified by additional observations.

The results could facilitate the understanding of cloud formation and development. Clouds, such as convective clouds, can develop and expand extraordinarily fast under strong synoptic forcing or unstable conditions. Fog can be viewed as a kind of near-surface stratus cloud, which usually forms under stable conditions with weak synoptic forcings. However, as revealed in this study, it can also develop and propagate fast under the effect of BLLJ. The quantitative relations between

301 BLLJ and fog fast propagation may have implications on the cloud formation and development mechanism under stable
302 synoptic conditions.

303 5. Conclusions

304 Previous studies have found that the spatial propagation of fog could be rather fast under favourable conditions, and the
305 boundary layer low-level jet (BLLJ) could be a potential reason. In this study, we analyze the fast spatial propagation fea-
306 ture of a large-scale fog event in Jiangsu Province, China by high spatiotemporal resolution ground and satellite observa-
307 tions. The key impact factors and mechanisms of the BLLJ effect on fast spatial propagation are quantitatively revealed by
308 WRF model simulations. Results show that:

309 The fog initials at 22:00 on 20 January 2020 over Jiangsu coastal area, and it reaches the west boundary of Jiangsu at 07:00
310 next day. Satellite retrievals show that the southeast side of fog area varies slightly but the northwest side expands fast,
311 with the maximum propagation speed of 9.6m/s. During the fog period, the ground wind direction is consistent with fog
312 propagation, which favours the vapor transportation from ocean and promotes fog formation. However, the wind speed
313 ($<3\text{m/s}$) is at least one-third less than the fog propagation speed. Therefore, the ground meteorologies are insufficient to
314 explain the fast propagation of fog. The influencing factors and mechanisms need to be investigated by exploring the PBL
315 characteristics through numerical simulations.

316 The WRF model well simulates the temporal variation of meteorologies and reproduces the spatiotemporal evolution of
317 fog area. A BLLJ ($>6\text{m/s}$) exists at the height between 50 and 500m. The jet core occurs at 1000hpa (200m) with the
318 southeasterly winds of 10m/s, which can fit the propagation direction and speed of fog. Therefore, the southeasterly BLLJ
319 is hypothesized to be the cause of fast propagation. BLLJ creates favourable PBL conditions by transporting moisture and
320 warm air from ocean. The moisture advection and the vapor turbulent mixing generated by wind speed shear increase the
321 humidity within PBL, and the propagation of fog area coincides with the movement of high humidity zone (vapor mixing
322 ratio $>4\text{g/kg}$). The warm advection from ocean deepens inversion layer and additionally favours the accumulation of mois-
323 ture and condensation nuclei. Additionally, it is found that ~~fog-low stratus~~ could ~~firstly~~ form ~~at upper layer~~ above surface
324 and subsides to be ground fog within 0~20min. The moisture advection is also responsible for the formation of low stra-
325 tusupper level fog.

326 Sensitive experiments quantitatively reveal the contributions of moisture advection and temperature advection to fog
327 propagation. When moisture (temperature) advection is turned off, the fog area decreases by 62% (50%) and the propaga-
328 tion speed decrease by about 4.6m/s (5.2m/s). Process analysis on fog liquid water content (LWC) further illustrates the
329 mechanism of fog propagation. Condensation (Cond) and LWC turbulent exchange (Vmix) are two important physical
330 processes. At upper level (30~200m), Cond is positive and Vmix is negative. It indicates that BLLJ-related moisture ad-
331 vection significantly promotes condensation and probably favours ~~fog-low stratus~~ formation-at upper level. At ground and
332 lower level (0~30m), Cond is basically negative and Vmix is positive. It indicates that ~~fog-cloud~~ droplets at upper level are
333 entrained downward by turbulent mixing, leading to the subsequent formation of ground fog. The ~~subsidence of up-~~
334 ~~per level fog to ground~~ stratus lowering phenomenon needs to be verified by additional observations.

335 In this study, by combination of observations and simulations, we have revealed the effect of southeasterly BLLJ on fog
336 propagation, and quantified the contributions of BLLJ-related moisture advection and temperature advection to fog propa-
337 gation. Three possible mechanisms are concluded: 1) Moisture advection from ocean promotes vapor condensation in
338 downstream area, which could be the dominant cause; 2) Warm advection from ocean deepens inversion layer and addi-
339 tionally promote vapor accumulation within PBL. 3) The moisture advection probably promotes upper-level fog/low stratus
340 formation first, and later it subsides to be ground fog by turbulent mixing of fog-cloud droplets. The coexistence of fast fog
341 propagation and BLLJ is not a common phenomenon, so finding more cases requires additional work. It should be ad-
342 dressed in future studies in order to deeply understand the relationships between fog propagation and BLLJ under different
343 regions and synoptic conditions. Their quantitative relationships could facilitate the understanding of cloud formation and
344 development under stable synoptic conditions, since fog can be viewed as near-surface stratus cloud that can potentially
345 propagate fast under stable conditions.

346

347 *Code and data availability.* Some of the data repositories have been listed in Section 2. The other data, model outputs and
348 codes can be accessed by contacting Duanyang Liu via liuduanyang2001@126.com.

349 *Author contributions.* SY performed the model simulation, data analysis and manuscript writing. HW and DL proposed the
350 idea, supervised this work and revised the manuscript. XL helped the revision of the manuscript. FZ provided and analyzed
351 the observation data.

352 *Competing interests.* The authors declare that they have no conflict of interest.

353 *Acknowledgements.* This work is supported by the Special Project of Innovative Development of CMA (CXFZ2023J022),
354 Open Research Foundation of Jiangsu Marine Meteorology (HYQX2022), Beijige Foundation (BJG202307), Research
355 Foundation of Jiangsu Meteorology Bureau (KM202307), Basic Research Fund of CAMS (2022Y025).

356

357 **References**

- 358 Andreas, E.L., Claffy, K.J., and Makshtas, A.P.: Low-level atmospheric jets and inversions over the western Weddell Sea,
359 *Boundary Layer Meteorol*, 97(3), 459–486, <https://doi.org/10.1023/A:1002793831076>, 2000.
- 360 Bott, A.: On the influence of the physico-chemical properties of aerosols on the life cycle of radiation fogs, *J. Aerosol Sci*,
361 21(1-2), 1–31, <https://doi.org/10.1007/BF00119960>, 1991.
- 362 Boutle, I., Price, J., Kudzotsa, I., Kokkola, H., and Romakkaniemi, S.: Aerosol-fog interaction and the transition to well-mixed
363 radiation fog, *Atmos. Chem. Phys.*, 18(11), 1–19, <https://doi.org/10.5194/acp-18-7827-2018>, 2017.
- 364 Cermak, J. and Bendix, J.: A novel approach to fog/low stratus detection using Meteosat 8 data, *Atmos. Res.*, 87(3-4), 279–292,
365 <https://doi.org/10.1016/j.atmosres.2007.11.009>, 2008.
- 366 Dhangar, N. G., Lal, D. M., Ghude, S. D., Kulkarni, R., and Rajeevan, M.: On the conditions for onset and development of fog
367 over new delhi: an observational study from the wifex, *Pure Appl. Geophys*, 673, 1-20,
368 <https://doi.org/10.1007/s00024-021-02800-4>, 2021.
- 369 Dorman, C.E., Hoch, S.W., Gultepe, I., Wang, Q., Yamaguchi, R., Fernando, H., Krishnamurthy, R.: Large-Scale Synoptic Sys-
370 tems and Fog During the C-FOG Field Experiment. *Boundary-Layer Meteorol*, 181, 171–202,
371 <https://doi.org/10.1007/s10546-021-00641-1>, 2021.

372 Dupont, J., Haeffelin, M., Protat, A., Bouniol, D., Boyouk, N., and Morille, Y.: Stratus–Fog Formation and Dissipation: A 6-Day
373 Case Study, *Boundary-Layer Meteorol*, 143, 207–225, <https://doi.org/10.1007/s10546-012-9699-4>, 2012.

374 Di Vittorio, A. V. and Emery, W. J.: An automated, dynamic threshold cloud-masking algorithm for daytime AVHRR images over
375 land, *IEEE Trans. Geosci*, 40, 1682–1694, <https://doi.org/10.1109/TGRS.2002.802455>, 2002.

376 Fathalli, M., Lac, C., Burneta, F., and Vié, B.: Fog due to stratus lowering: Experimental and modelling case study, *Q. J. R. Me-*
377 *eteorol*, 148(746), 2299–2324. <https://doi.org/10.1002/qj.4304>, 2022.

378 Gao, S., Lin, H., Shen, B., and Fu, G.: A heavy sea fog event over the Yellow Sea in March 2005: Analysis and numerical mod-
379 eling, *Adv Atmos Sci*, 24, 65-81, <https://doi.org/10.1007/s00376-007-0065-2>, 2007.

380 Gao, Y., Liu, D., Yan, S., Zhou, W., Wang, H., Zu, F., Mei, Q., Yi, C., and Sheng, Y.: Influence of sea-land breeze on formation
381 and dissipation of severe dense fog and its explosive enhancement in the Yellow Sea Coastal Area, *Sci. China Earth Sci.*,
382 2023. (accepted; under translation into English)

383 Gultepe, I., Tardif, R., Michaelides, S. C., Cermak, J., Bott, A., Bendix, J., Muller, M. D., et al.: Fog research: a review of past
384 achievements and future perspectives, *Pure Appl. Geophys*, 164, 1121–1159, <https://doi.org/10.1007/s00024-007-0211-x>,
385 2007.

386 Haeffelin, M., Bergot, T., Elias, T., Tardif, R., Carrer, D., Chazette, P., and Zhang, X.: PARISFOG: Shedding new light on fog
387 physical processes, *Bull Am Meteorol Soc*, 91(6), 767-783, <https://doi.org/10.1175/2009bams2671.1>, 2010.

388 Jia, X., Quan, J., Zheng, Z., Liu, X., Liu, Q., He, H., and Liu, Y.: Impacts of anthropogenic aerosols on fog in North China Plain,
389 *J. Geophys. Res.-Atmos.*, 124, 252–265, <https://doi.org/10.1029/2018jd029437>, 2018.

390 Jiao, S., Zhu, C., Zhu, Y., Yuan, C., Zu, F., and Sun, K.: A discussion on the reason for a rare persistent heavy fog event in Jiang-
391 su Province, *Acta Meteorol. Sin.*, 74, 200–212, <https://doi.org/10.11676/qxxb2016.015>, 2016.

392 Koračin, D., Dorman, C. E., Lewis, J. M., Hudson, J. G., Wilcox, E. M., and Torregrosa, A.: Marine fog: A review, *Atmos. Res.*,
393 143, 142-175, <https://doi.org/10.1016/j.atmosres.2013.12.012>, 2014.

394 Korb, G. and Zdunkowski, W.: Distribution of radiative energy in ground fog, *Tellus*, 22(3), 298-320,
395 <https://doi.org/10.3402/tellusa.v22i3.10223>, 1970.

396 Kraus, H., Malcher, J., and Schaller, E.: A nocturnal low level jet during PUKK, *Boundary Layer Meteorol*, 31, 187-195,
397 <https://doi.org/10.1007/BF00121177>, 1985.

398 Kunkel, B. A.: Parameterization of Droplet Terminal Velocity and Extinction Coefficient in Fog Models, *J. Appl. Meteorol*, 23(1),
399 34–41, [https://doi.org/10.1175/1520-0450\(1984\)023<0034:PODTVA>2.0.CO;2](https://doi.org/10.1175/1520-0450(1984)023<0034:PODTVA>2.0.CO;2), 1983.

400 Li, P. and Fu, G.: The Formation Mechanism of a Spring Sea Fog Event over the Yellow Sea Associated with a Low-Level Jet,
401 *Weather and Forecasting*, 27(6), 1538-1553, <https://doi.org/10.1175/WAF-D-11-00152.1>, 2012.

402 Li, Z. H., Liu, D. Y., Yang, J.: The microphysical processes and macroscopic conditions of the radiation fog droplet spectrum
403 broadening, *Chinese J. Atmospheric Sci.*, 35, 41–54, <https://doi.org/10.3878/j.issn.1006-9895.2011.01.04>, 2011. (in Chinese)

404 Li, Z., Liu, D., Yan, W., Wang, H., Zhu, C., Zhu, Y., and Zu, F.: Dense fog burst reinforcement over Eastern China: A review,
405 *Atmos. Res.*, 230(D19), 104639, <https://doi.org/10.1016/j.atmosres.2019.104639>, 2019.

406 Liu, D., Yang, J., Niu, S., and Li, Z.: On the Evolution and Structure of a Radiation Fog Event in Nanjing, *Adv Atmos Sci*, 28(1),
407 223-237, <https://doi.org/10.1007/s00376-010-0017-0>, 2011.

408 Liu, D. Y., Niu, S. J., Yang, J., Zhao L., Lv, J., and Lu, C.: Summary of a 4-year fog field study in Northern Nanjing, part 1: fog
409 boundary layer, *Pure Appl. Geophys*, 169, 809–819, <https://doi.org/10.1007/s00024-011-0343-x>, 2012.

410 Liu, D., Yan, W., Yang, J., Pu, M., Niu, S., Li, Z.: A Study of the Physical Processes of an Advection Fog Boundary Layer,
411 *Boundary Layer Meteorol*, 158(1), 125-138, <https://doi.org/10.1007/s10546-015-0076-y>, 2016.

412 Liu, D., Li, Z., Yan, W., and Li, Y.: Advances in fog microphysics research in China, *Asia Pac J Atmos Sci*, 53(1), 131–148,
413 <https://doi.org/10.1007/s13143-016-0028-6>, 2017.

414 Liu, Q., Wang, Z. Y., Wu, B. G., Liu, J. L., and Gultepe, I.: Microphysics of fog bursting in polluted urban air, *Atmospheric En-*
415 *viron.*, 10, 118357, <https://doi.org/10.1016/j.atmosenv.2021.118357>, 2021.

416 Nakanishi, M.: Large-eddy simulation of radiation fog. *Boundary Layer Meteorol*, 94, 461-493,
417 <https://doi.org/10.1023/A:1002490423389>, 2000.

418 Pleim, J. E., Gilliam, R.: An indirect data assimilation scheme for deep soil temperature in the Pleim-Xiu land surface model, *J.*
419 *Appl. Meteorol*, 48, 1362-1376, <https://doi.org/10.1175/2009JAMC2053.1>, 2009.

420 Pu, M. J., Zhang, G. Z., Yan, W. L., and Li, Z. H.: Features of a rare advection-radiation fog event, *Sci. China Earth Sci.*, 51(7),
421 1044–1052, <https://doi.org/10.1007/s11430-008-0071-y>, 2008.

422 Quan, J., Liu, Y., Jia, X., Liu, L., Dou, Y., Xin, J., and Seinfeld, J. H.: Anthropogenic aerosols prolong fog lifetime in China, *Environ. Res. Lett.*, 16(4), 044048, <https://doi.org/10.1088/1748-9326/abef32>, 2021.

423 Schwenkel, J. and Maronga, B.: Large-eddy simulation of radiation fog with comprehensive two-moment bulk microphysics:
424 impact of different aerosol activation and condensation parameterizations, *Atmos. Chem. Phys.*, 19(10), 1-23,
425 <https://doi.org/10.5194/acp-19-7165-2019>, 2018.

427 Shao, N., Lu, C., Jia, X., Wang, Y., Li, Y., Yin, Y., Zhu, B., Zhao, T., Liu, D., Niu, S., Fan, S., Yan, S., and Lv, J.: Radiation fog
428 properties in two consecutive events under polluted and clean conditions in the Yangtze River Delta, China: a simulation
429 study, *Atmos. Chem. Phys.*, 23, 9873–9890, <https://doi.org/10.5194/acp-23-9873-2023>, 2023.

430 Shen, P., Liu, D., Gultepe, I., Lin, H., Cai, N., and Cao, S.: Boundary layer features of one winter fog in the Yangtze River Delta,
431 China, *Pure Appl. Geophys.*, 179(9), 3463-3480, <https://doi.org/10.1007/s00024-022-03119-4>, 2022.

432 Steeneveld, G. J., Ronda, R. J., and Holtslag, A. A. M.: The Challenge of Forecasting the Onset and Development of Radiation
433 Fog Using Mesoscale Atmospheric Models, *Boundary Layer Meteorol.*, 154(2), 265–289,
434 <https://doi.org/10.1007/s10546-014-9973-8>, 2014.

435 Sukoriansky, S., Galperin, B., Perov, V.: Application of a new spectral model of stratified turbulence to the atmospheric boundary
436 layer over sea ice, *Boundary Layer Meteorol.*, 117, 231–257, <https://doi.org/10.1007/s10546-004-6848-4>, 2005.

437 Tian, M., Wu, B., Huang, H., Zhang, H., Zhang, W., and Wang, Z.: Impact of water vapor transfer on a Circum-Bohai-Sea heavy
438 fog Observation and numerical simulation, *Atmos. Res.*, 229, 1-22, <https://doi.org/10.1016/j.atmosres.2019.06.008>, 2019.

439 van der Velde, I. R., Steeneveld, G. J., Wichers Schreur, B. G. J., and Holtslag, A. A. M.: Modeling and Forecasting the Onset
440 and Duration of Severe Radiation Fog under Frost Conditions, *Mon Weather Rev.*, 138(11), 4237–4253,
441 <https://doi.org/10.1175/2010mwr3427.1>, 2010.

442 Wang, H., Zhang, Z., Liu, D., Zhu, Y., Zhang, X., and Yuan, C.: Study on a Large-Scale Persistent Strong Dense Fog Event in
443 Central and Eastern China, *Adv. Meteorol.*, 4, 1–15, <https://doi.org/10.1155/2020/8872334>, 2020.

444 Wang, Y., Lu, C., Niu, S., Lv, J., Jia, X., Xu, X., et al.: Diverse dispersion effects and parameterization of relative dispersion in
445 urban fog in eastern China, *J. Geophys. Res.-Atmos.*, 128, e2022JD037514, <https://doi.org/10.1029/2022JD037514>, 2023.

446 Wei, W., Zhang, H. S., Ye, X. X.: Comparison of low-level jets along the north coast of China in summer, *J. Geophys.*
447 *Res.-Atmos.*, 119(16), 9692–9706, <https://doi.org/10.1002/2014JD021476>, 2014.

448 Wobrock, W., Schell, D., Maser, R., Kessel, M., Jaeschke, W., Fuzzi, S., and Bendix, J.: Meteorological characteristics of the Po
449 Valley fog, *Tellus B*, 44(5), 469-488, <https://doi.org/10.3402/tellusb.v44i5.15562>, 1992.

450 Wu, B., Li, Z., Ju, T., and Zhang, H.: Characteristics of Low-level jets during 2015–2016 and the effect on fog in Tianjin, *Atmos.*
451 *Res.*, 245, 105102, <https://doi.org/10.1016/j.atmosres.2020.105102>, 2020.

452 Yan, S., Zhu, B., Zhu, T., Shi, C., Liu, D., Kang, H., Lu, W., and Lu, C.: The effect of aerosols on fog lifetime: observational ev-
453 idence and model simulations, *Geophys. Res. Lett.*, 48(2), e2020GL61803, <https://doi.org/10.1029/2020GL091156>, 2021.

454 Yang, Y., Hu, X.-M., Gao, S., and Wang, Y.: Sensitivity of WRF simulations with the YSU PBL scheme to the lowest model level
455 height for a sea fog event over the Yellow Sea, *Atmos. Res.*, 215, 253–267, <https://doi.org/10.1016/j.atmosres.2018.09.004>,
456 2019.

457 Ye, X., Wu, B., and Zhang, H.: The turbulent structure and transport in fog layers observed over the Tianjin area, *Atmos. Res.*,
458 153, 217-234, <https://doi.org/10.1016/j.atmosres.2014.08.003>, 2015.

459 Zhang, G., Bian, L., Wang, J., Yang, Y., Yao, W., and Xu, X.: The boundary layer characteristics in the heavy fog formation pro-
460 cess over Beijing and its adjacent areas, *Sci. China Earth Sci.*, 48, 88-101, <https://doi.org/10.1360/05yd0029>, 2005.

461 [Zhou, B. and Ferrier, B.: Asymptotic Analysis of Equilibrium in Radiation Fog, *J. Appl. Meteorol. and Climatology*, 47,](https://doi.org/10.1175/2007JAMC1685.1)
462 [1704-1722, https://doi.org/10.1175/2007JAMC1685.1, 2008.](https://doi.org/10.1175/2007JAMC1685.1)

463 [Zhou, B. and Du, J.: Fog prediction from a multimodel mesoscale ensemble prediction system, *Weather and Forecasting*, 25\(1\),](https://doi.org/10.1175/2009WAF2222289.1)
464 [303-322, https://doi.org/10.1175/2009WAF2222289.1, 2010.](https://doi.org/10.1175/2009WAF2222289.1)

465 [Zhou, B., Du, J., Gultepe, I., and Dimego, G.: Forecast of low visibility and fog from NCEP: Current status and efforts, *Pure*](https://doi.org/10.1007/s00024-011-0327-x)
466 [Appl. Geophys., 169, 895-909, https://doi.org/10.1007/s00024-011-0327-x, 2012.](https://doi.org/10.1007/s00024-011-0327-x)

467 Zhu, Y., Zhu, C., Zu, F., Wang, H., Liu Q., Qi, M., and Wang, Y.: A persistent fog event involving heavy pollutants in Yancheng
468 area of Jiangsu Province, *Adv. Meteorol*, 2018, 2512138, <https://doi.org/10.1155/2018/2512138>, 2018.
469 Zhu, Y., Li, Z., Zu, F., Wang, H., Liu, Q., Qi, M., and Wang, Y.: The propagation of fog and its related pollutants in the Central
470 and Eastern China in winter, *Atmos. Res.*, 265, 105914, <https://doi.org/10.1016/j.atmosres.2021.105914>, 2022.
471

472 Table 1. Model parameterization schemes and sensitive experiments

Physical scheme	Option
Boundary layer	QNSE
Microphysics	Lin double moment
Longwave radiation	RRTM
Shortwave radiation	Goddard
Land surface	Pleim-Xiu
Cumulus	Grell-3D
Grid nudging	Off
Observation nudging	Off
Experiment	Description
Base	The base condition
Tadv0	Turning off temperature advection
QvAdv0	Turning off water vapor advection
QcAdv0	Turning off fog-cloud water advection
NoAdv	Turning off all advectons above

473

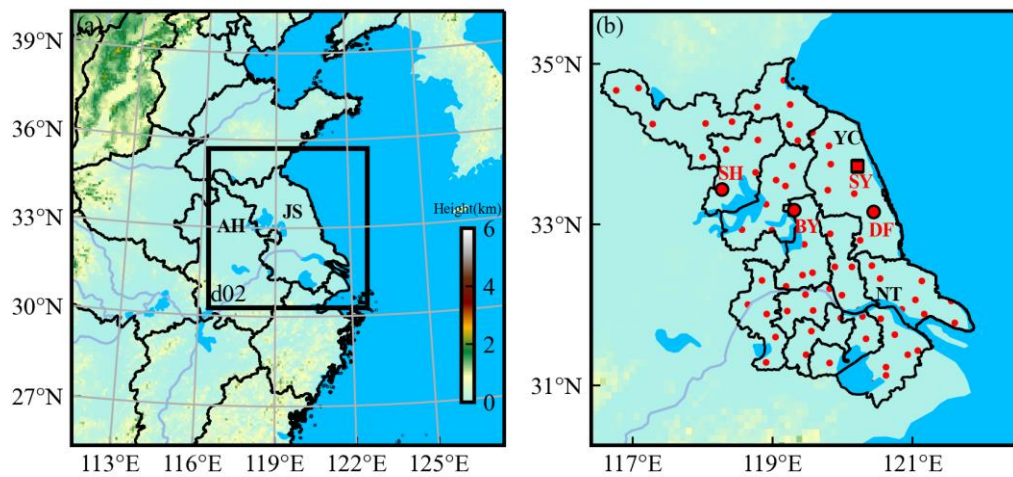
474 Table 2. The times when visibility reaches 1000m, 500m and 200m at three representative stations. (DF:Dafeng,
475 BY:Baoying, SH:Sihong).

Station	Location	Formation (Vis=1000m)		Vis=500m		Vis=200m	
		Time	Wind	Time	Wind	Time	Wind
DF	120.48°E,33.20°N	19:45	1.3m/s, E	22:55	1.2m/s, E	23:45	1.3m/s, E
BY	119.30°E,33.23°N	01:25	1.2m/s, ESE	03:15	1.4m/s, ESE	03:45	1.3m/s, SE
SH	118.22°E,33.48°N	04:50	1.6m/s, ESE	06:10	1.3m/s, ESE	07:15	2.4m/s, ESE
	Distance (km)	Time difference (h)		Time difference (h)		Time difference (h)	
DF-BY	110	4.7		4.3		4.0	
BY-SH	105	3.4		2.9		3.5	

476

477

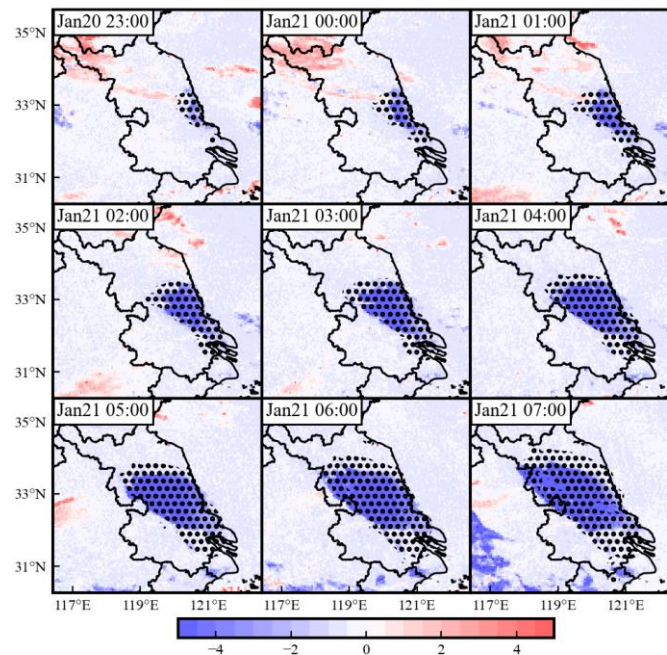
478



480

481 Figure 1. The parent and nest model domain. The shaded color is terrain height. The red points are automatic weather stations
 482 in Jiangsu, China. ~~The; and the~~ three larger circle points are Sihong (SH), Baoying (BY), and Dafeng (DF) stations, and the
 483 square point is Sheyang (SY) sounding station. The black labels are some province or city names. (JS:Jiangsu Province;
 484 AH:Anhui Province; YC:Yanchen; NT:Nantong).

485

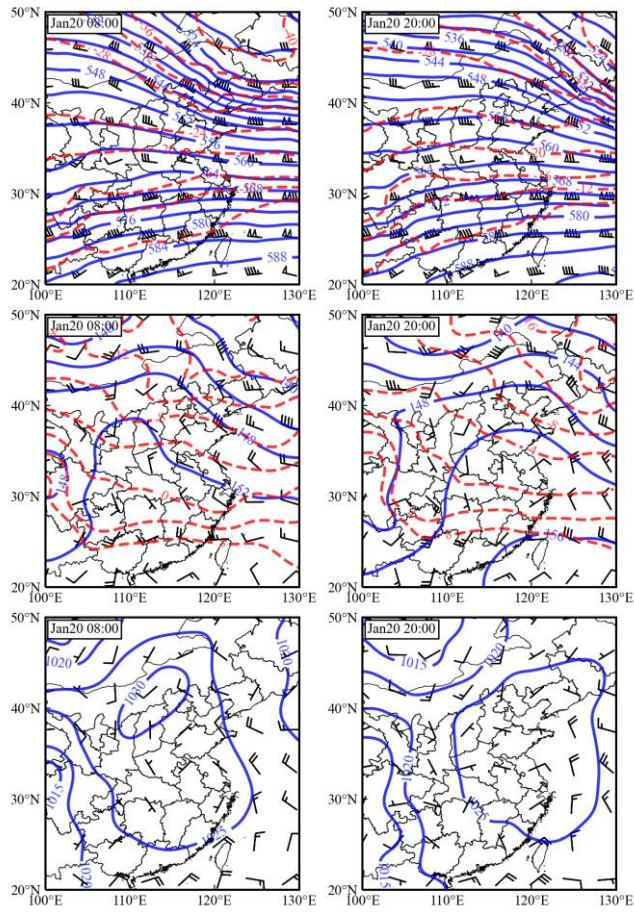


486

487 Figure 2. The spatial evolution of fog. The black dots are simulated fog areas. The shaded colors are satellite observed bright-
 488 ness temperature difference ($3.9\mu\text{m}$ minus $11.2\mu\text{m}$), where the blue colors (smaller than -2 K) indicate the fog areas.

489

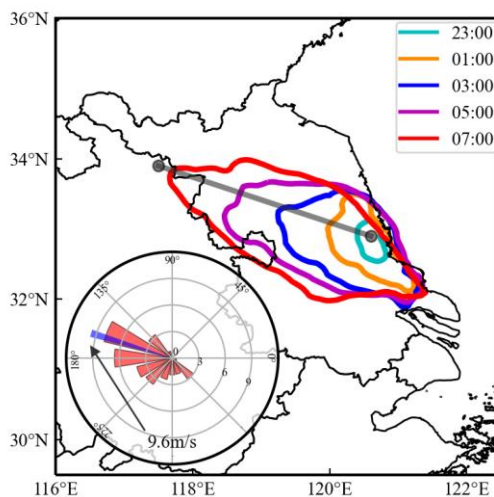
490



491

492 Figure 3. The synoptic background of 500hpa (first row), 850hpa (second row) and surface (third row) at 08:00 and 20:00 on
 493 20 January 2020.

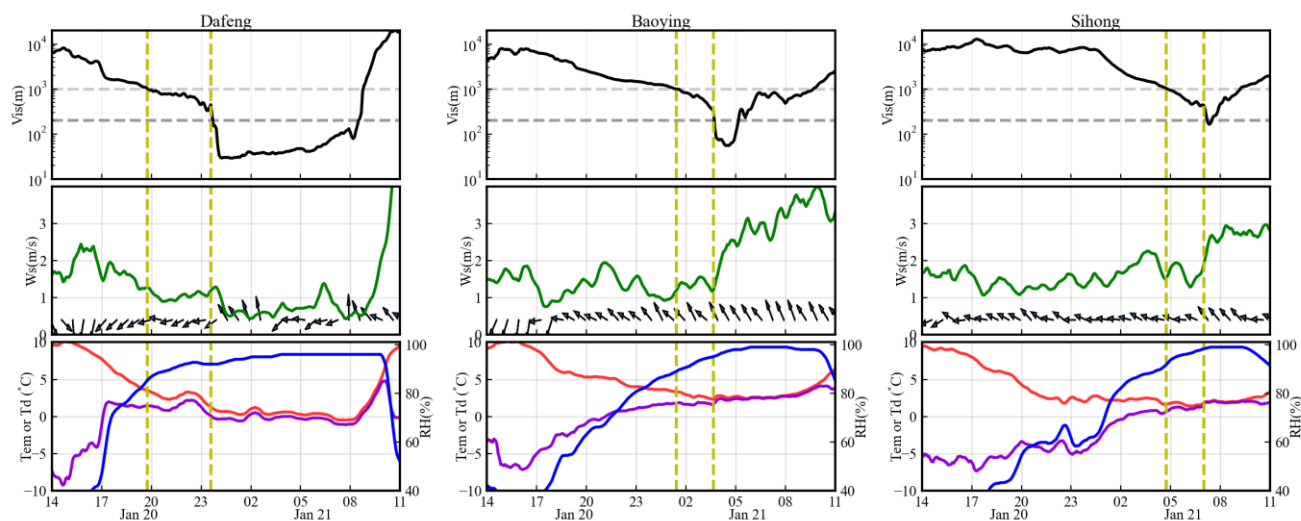
494



496

497 Figure 4. The colored curves are the fog boundaries (satellite retrievals) from 23:00 on 20 January to 07:00 next day every 2
 498 hours. The gray straight line indicates the fog propagation direction, and the vertical features of meteorologies at this line will be
 499 analyzed in Figures 7, 8, and 9. The lower-left polar plot is the fog propagation speed at 16 directions (22.5° interval), and the
 500 narrow blue bar highlights the maximum propagation speed (9.6m/s) occurring at 160° direction (in Cartesian coordinate system)
 501 (from southeast to northwest).

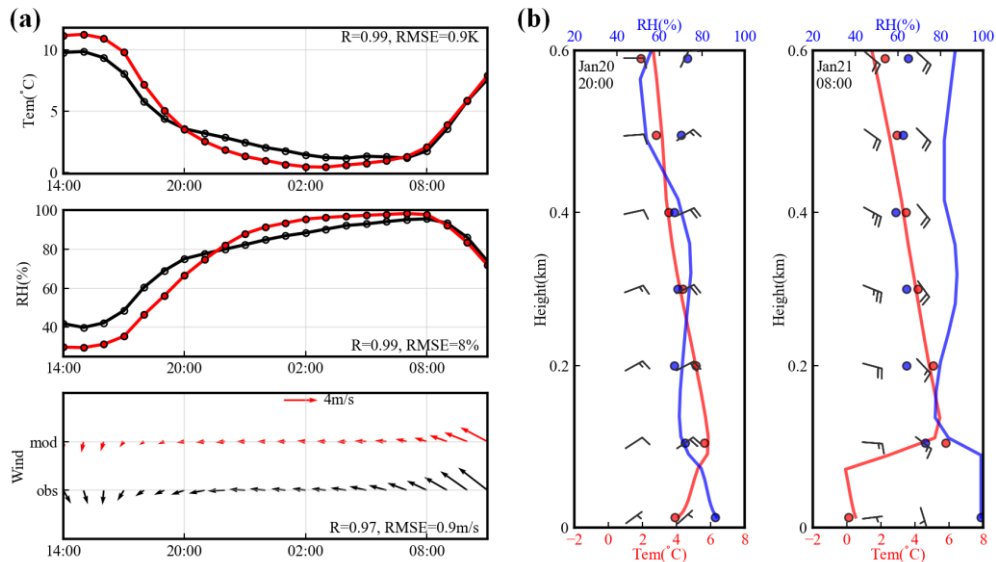
502



503

504 Figure 5. The temporal variation of ground visibility (Vis ; black line), wind speed (Ws ; green line), wind direction (vectors),
 505 temperature (Tem ; red line), dew point (Td ; violet line) and relative humidity (RH ; blue line) at Dafeng, Baoying, and Sihong
 506 stations. The horizontal dashed lines are visibilities of 1000m and 200m. The vertical dashed lines mark the times of fog for-
 507 mation and visibility burst dropping.

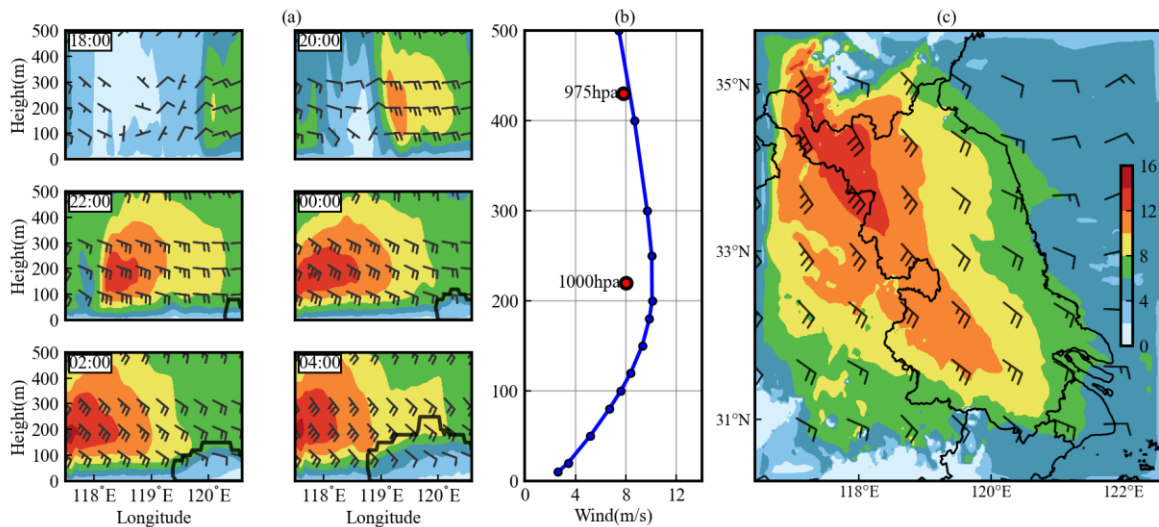
508



510

511 Figure 6. (a) The model performance on 2m Temperature (Tem), 2m Relative humidity (RH) and 10m wind speed and direction.
 512 The red color is simulation and black color is observation. The time is from 14:00 on 20 January 2020 to 11:00 next day. (b) The
 513 model performance on temperature (red), RH (blue) and wind (barbs) profiles at Sheyang sounding station. For temperature and
 514 RH, the observations are scatters and simulations are solid lines. For wind barbs, the left column is observations and the right
 515 column is simulations. The scatters and barbs are interpolated onto 0~600m every 100m.

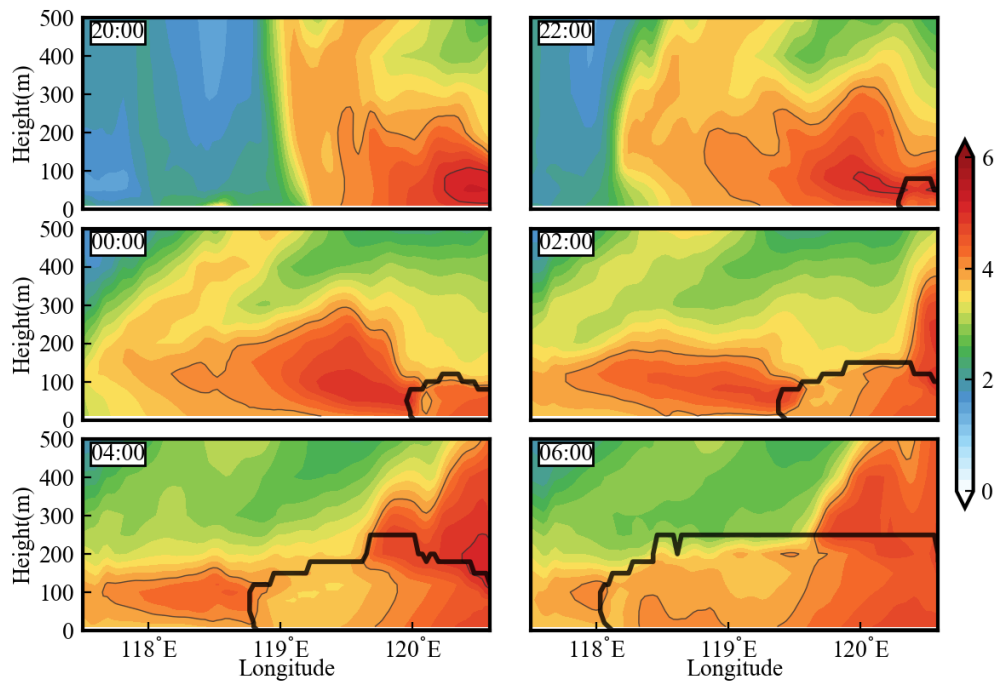
516



517

518 Figure 7. (a) The height-longitude variation of horizontal wind direction (vectors) and wind speed (shaded colors) at the cross-
 519 ing line in Figure 4. The lower-right black polygons are the fog area. The times are from 18:00 on 20 January to 04:00 next day.
 520 (b) The averaged wind speed profile at the crossing line during 23:00~07:00. The two red points are the wind speed calculated
 521 from ERA5 reanalysis. (c) The averaged wind direction (vectors) and wind speed (shaded colors) at 1000hpa during
 522 23:00~07:00.

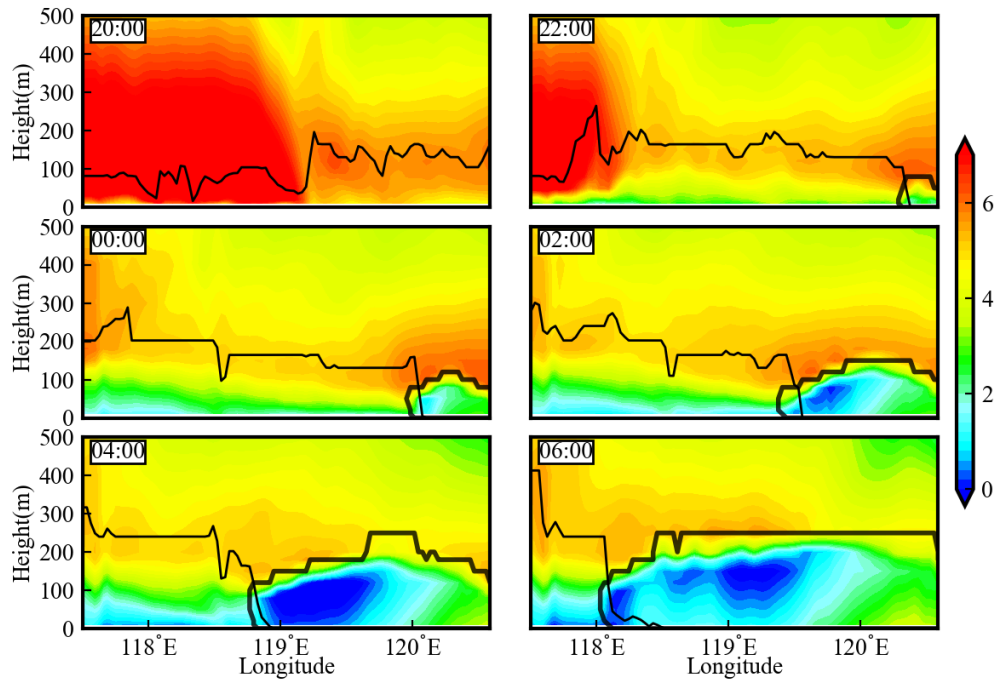
523



524

525 Figure 8. The height-longitude distribution of water vapor mixing ratio (g/kg) at the crossing line in Figure 4. The deep black
 526 polygons are the fog area. The light black lines are the region of water vapor mixing ratio larger than 4g/kg. The times are from
 527 20:00 on 20 January to 06:00 next day.

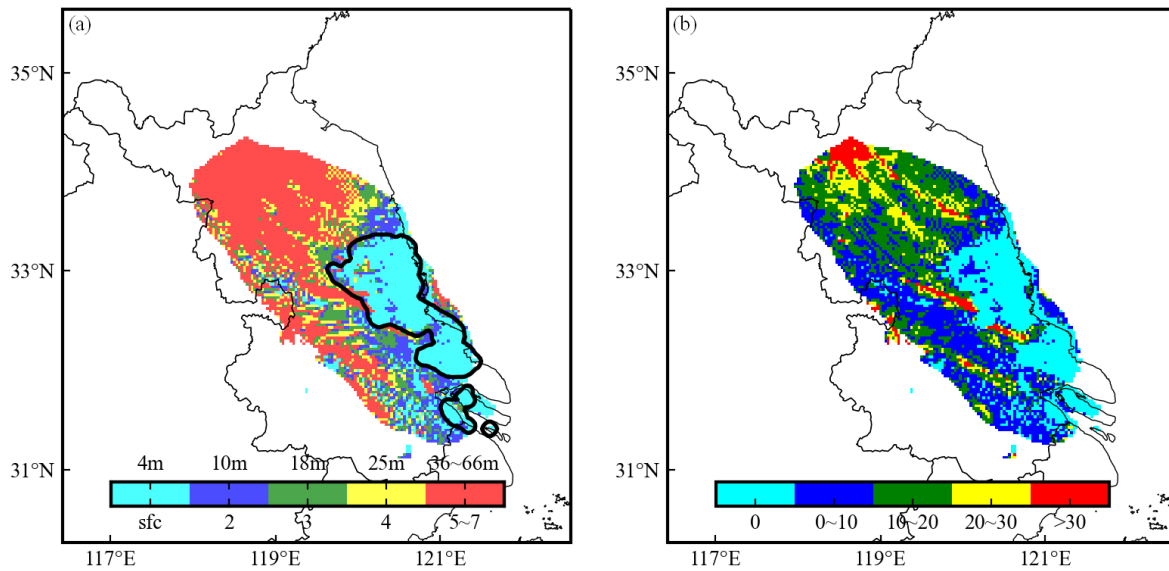
528



529

530 Figure 9. Same as the previous figure, but for the temperature. The bold black polygons are the fog area. The thin black lines
 531 are the top of inversion layer.

532



533

534

535

536

537

538

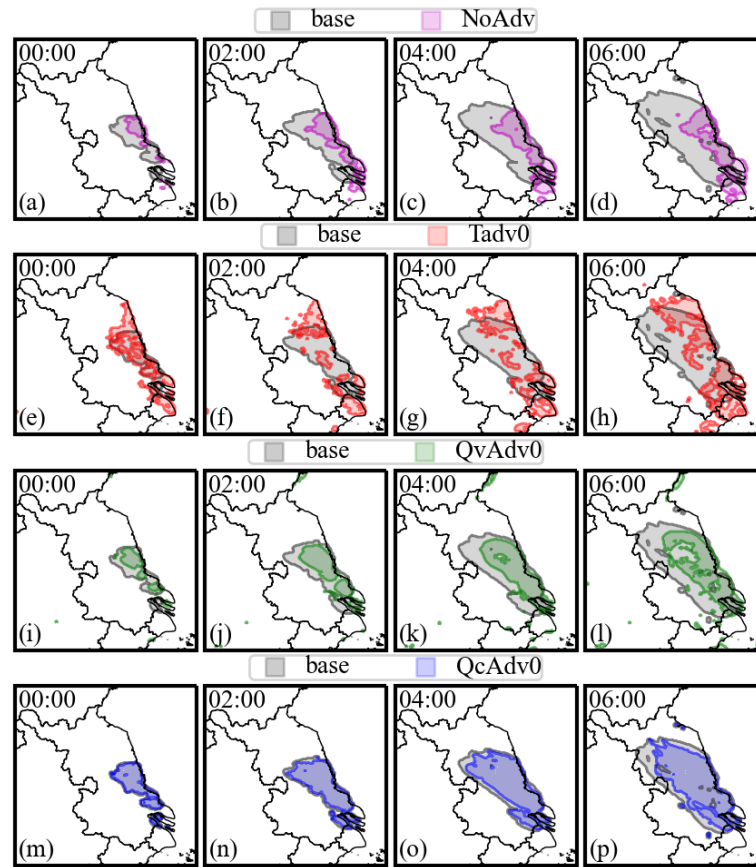
539

540

541

542

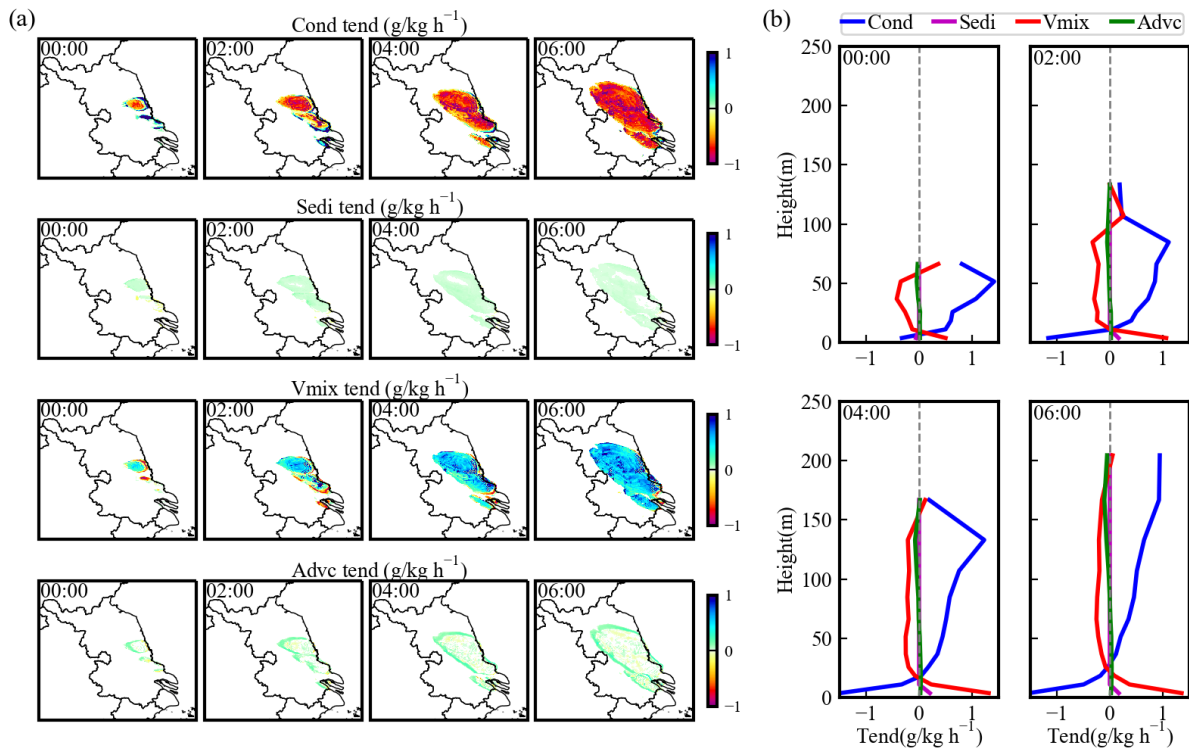
Figure 10. (a) The height (shaded color) at which fog/low stratus firstly forms. The black contours are the ground fog areas at 00:00 on 21 January 2020. The colorbar represents the model level and the corresponding height above surface. For example, the cyan colors indicate that fog firstly forms at the surface level with the corresponding height of about 4m. The red colors indicate that low stratus fog firstly forms at the 5th to 7th model level with the corresponding height of about 36~66m. (b) The time differences between ground fog formation and upper-level fog/low stratus formation. For example, the cyan colors indicate that fog firstly forms at ground. The blue colors indicate that the ground fog forms 0~10min later than the upper-level fog/low stratus formation.



544

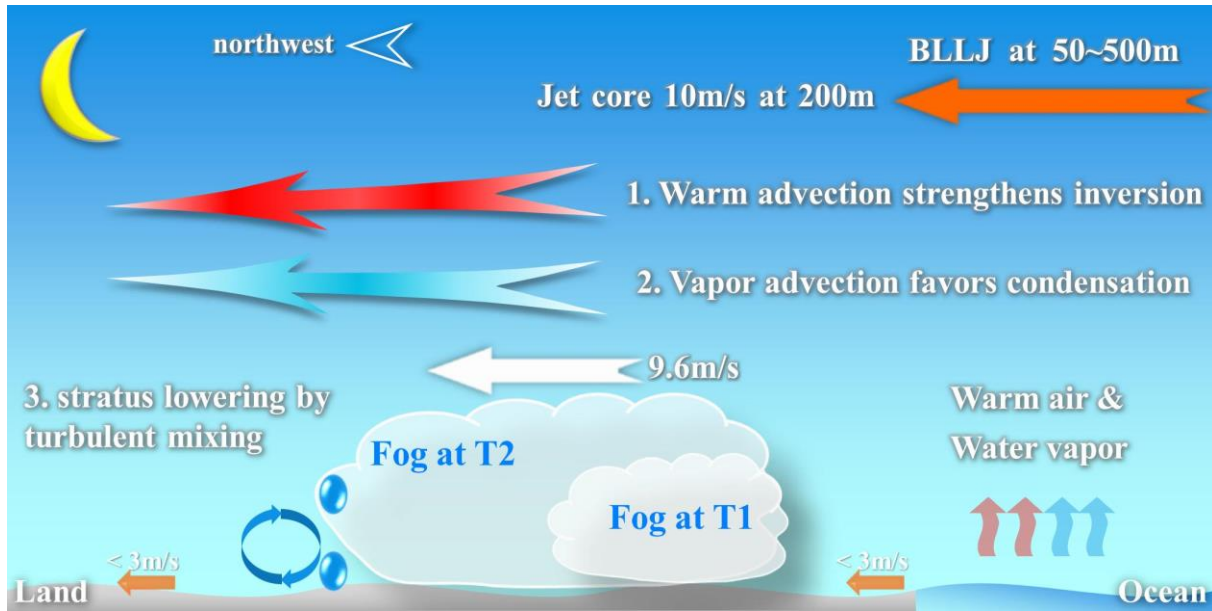
545 Figure 11. The temporal variation of ground fog area under different experiments from 00:00 to 06:00 on 21 January. The black
 546 color is the base experiment. The Tadv0 (red), QvAdv0 (green) and QcAdv0 (blue) are the experiments turning off temperature
 547 advection, moisture advection and fogcloud water advection, respectively. The NoAdv (pink) is the experiment turning off all of
 548 the above advections.

549



551

552 Figure 12. (a) The spatial distribution of the four process tendencies contributing to LWC variation at ground level. (b) The
 553 vertical profiles of the process tendencies averaged in fog area. The times are from 00:00 to 06:00 on 21 January.
 554 (Cond:condensation or evaporation; Sedi:sedimentation; Vmix:turbulent exchange; Advc:horizontal and vertical advection).
 555



557

558 Figure 13. The concept diagram of fog propagation. The ground wind speed (short orange arrows) is generally less than 3m/s.
 559 A southeasterly BLLJ exists at the height from 50 to 500m, and the jet core intensity is 10m/s at 200m (the long orange arrow).
 560 The updraft arrows represent the warm and wet air from ocean. The two cloud shapes are fog areas at two adjacent times, and the
 561 white arrow indicates the fog propagation speed (9.6m/s). The fog propagation is probably caused by three approaches: 1) Moisture
 562 advection from ocean promotes vapor condensation in the downstream area, which could be the dominant cause (the blue
 563 fancy arrow); 2) Warm advection from ocean deepens inversion layer and additionally promotes vapor accumulation within PBL
 564 (the red fancy arrow); 3) The moisture advection probably result in the upper-level fog/low stratus formation, and later it subsides
 565 to ground by turbulent mixing of fogcloud droplets (the blue water drops and circular arrows). Note that warm and moisture ad-
 566 vections occur at nearly all heights below 500m, not merely at the height indicated by arrows.